The Journal *of* Immunology

OX40L-JAG1–Induced Expansion of Lineage-Stable Regulatory T Cells Involves Noncanonical NF-κB Signaling

This information is current as of November 9, 2019.

Prabhakaran Kumar, Swarali Surendra Lele, Vandhana K. Ragothaman, Divya Raghunathan, Alan L. Epstein, Shigeru Chiba and Bellur S. Prabhakar

Supplementary Material	http://www.jimmunol.org/content/suppl/2019/11/07/jimmunol.1900530.DCSupplemental

Why *The JI*? Submit online.

- **Rapid Reviews! 30 days*** from submission to initial decision

- **No Triage!** Every submission reviewed by practicing scientists

- **Fast Publication!** 4 weeks from acceptance to publication

*average

Subscription	Information about subscribing to *The Journal of Immunology* is online at: http://jimmunol.org/subscription
Permissions	Submit copyright permission requests at: http://www.aai.org/About/Publications/JI/copyright.html
Email Alerts	Receive free email-alerts when new articles cite this article. Sign up at: http://jimmunol.org/alerts

OX40L-JAG1–Induced Expansion of Lineage-Stable Regulatory T Cells Involves Noncanonical NF-κB Signaling

Prabhakaran Kumar,* Swarali Surendra Lele,* Vandhana K. Ragothaman,* Divya Raghunathan,* Alan L. Epstein,[†] Shigeru Chiba,[‡] and Bellur S. Prabhakar*,[§]

Foxp3^{+}T regulatory cells (Tregs) control autoimmune response by suppressing proliferation and effector functions of self-reactive Foxp3^{−}CD4^{+}/CD8^{+} T cells and thereby maintain the critical balance between self-tolerance and autoimmunity. Earlier, we had shown that OX40L-JAG1 cosignaling mediated through their cognate receptors OX40 and Notch3 preferentially expressed on murine Tregs can selectively induce their proliferation in the absence of TCR stimulation. However, the differential molecular mechanisms regulating TCR-independent versus TCR-dependent Treg proliferation and lineage stability of the expanded Tregs remained unknown. In this study, we show that OX40L-JAG1 treatment induced TCR-independent proliferation of Tregs in the thymus and periphery. The use of Src kinase inhibitor permitted us to demonstrate selective inhibition of TCR-dependent T cell proliferation with little to no effect on OX40L-JAG1–induced TCR-independent Treg expansion in vitro, which was critically dependent on noncanonical NF-κB signaling. OX40L-JAG1–expanded Tregs showed sustained lineage stability as indicated by stable demethylation marks in Treg signature genes such as *Foxp3, Il2ra, Ctla4, Ikzf2,* and *Ikzf4.* Furthermore, OX40L-JAG1 treatment significantly increased CTLA4^{+} and TIGIT[+] Tregs and alleviated experimental autoimmune thyroiditis in mice. Relevance of our findings to humans became apparent when human OX40L and JAG1 induced TCR-independent selective expansion of human Tregs in thymocyte cultures and increased human Tregs in the liver tissue of humanized NSG mice. Our findings suggest that OX40L-JAG1–induced TCR-independent Treg proliferation is a conserved mechanism that can be used to expand lineage-stable Tregs to treat autoimmune diseases.   *The Journal of Immunology*, 2019, 203: 000–000.

T he CD4^{+}Foxp3^{+}T regulatory cells (Tregs) control autoimmune response by suppressing proliferation and/or effector functions of self-reactive CD4^{+}/CD8^{+} T cells, B cells, NK cells, and APCs, and thereby maintain self-tolerance (1, 2). Reduced Treg numbers and functions have been noted in many autoimmune diseases, including type 1 diabetes and autoimmune thyroiditis, and enhancing functional Foxp3^{+} Tregs has been shown to ameliorate these autoimmune diseases (3, 4). Despite conferring protection against autoimmune diseases (3, 5, 6),

the tendency of Tregs to lose lineage stability and morph into pathogenic effector T cells (Teffs) ("ex-Foxp3" cells) remains poorly understood and thus impedes clinical translation (7, 8). Treg-specific DNA demethylation (TSDR) at the *Foxp3* gene locus allows for the constitutive expression of *Foxp3*, which is essential for the repression of TCR activation–induced expression of inflammatory genes like *Ifn-g* and *Il-2* in Tregs (9). Additionally, Foxp3 expression alone is insufficient for optimal Treg function. CpG hypomethylation of *Il2ra* (*Cd25*), *Ctla4, Tnfrsf18* (*Gitr*), and *Ikzf4* (*Eos*) gene loci in natural Tregs (nTregs) represent a Foxp3-independent nTreg signature (8). Constitutive expression of these genes along with Foxp3 determines the lineage stability and optimum function of Tregs, and loss/reduced expression of these genes in Tregs can lead to impaired suppressive function (9).

Treg proliferation can occur through two different mechanisms: 1) Ag/TCR-dependent proliferation or 2) Ag/TCR-independent proliferation. Of these, TCR-dependent Treg proliferation is the most widely studied mechanism that requires two signals for proliferation. Recognition of MHC-bound antigenic peptides presented on APCs by the cognate TCRs expressed on the surface of Tregs acts as the primary activation signal. The secondary signal is provided by the interaction between costimulatory ligands, such as CD80/CD86, expressed on APCs with their cognate receptors, such as CD28 on Tregs (10). On the contrary, we and others have shown that Treg proliferation can be induced through an Ag/TCR-independent, but IL-2–dependent, mechanism by coculturing T cells with GM-CSF–derived, bone marrow–derived dendritic cells (11, 12). Further, we identified that cosignaling through two membrane-bound ligands (namely OX40L, which belongs to the TNFRSF, and Jagged 1 [JAG1], which belongs to Notch family ligands) expressed on GM-CSF–derived, bone marrow–derived dendritic cells is required and sufficient to cause TCR-independent Treg proliferation (13).

*Department of Microbiology and Immunology, University of Illinois College of Medicine, Chicago, IL 60612; [†]Department of Pathology, Keck School of Medicine at University of Southern California, Los Angeles, CA 900933; [‡]Department of Clinical and Experimental Hematology, Institute of Clinical Medicine, University of Tsukuba, Tsukuba 305-8575, Japan; and [§]Department of Ophthalmology, University of Illinois College of Medicine, Chicago, IL 60612

ORCIDs: 0000-0002-0657-6938 (P.K.); 0000-0001-7803-7338 (S.C.); 0000-0001-9815-9850 (B.S.P.).

Address correspondence and reprint requests to Dr. Bellur S. Prabhakar, Department of Microbiology and Immunology, University of Illinois College of Medicine, Room E-705 (M/C 790), 835 South Wolcott Avenue, Chicago, IL 60612. E-mail address: bprabhak@uic.edu

The online version of this article contains supplemental material.

Abbreviations used in this article: dLN, draining lymph node; DNMT, DNA methyltransferase; EAT, experimental autoimmune thyroiditis; JAG1, Jagged 1; NIK, NF-κB inducible kinase; nTreg, natural Treg; Tconv, conventional T cell; Teff, effector T cell; Treg, T regulatory cell; TSDR, Treg-specific DNA demethylation; WGBS, whole genome bisulfite sequencing.

The most commonly used ex vivo Treg expansion protocols rely on a TCR-dependent mechanism and use anti-CD3 and anti-CD28 mAbs to provide Ag receptor crosslinking and costimulatory signal. Although this is an effective approach for expanding Tregs, it can also cause concomitant proliferation of Teffs because of ubiquitous expression of CD3 and CD28 receptors on both Foxp3^{+} Tregs and Foxp3^{−} conventional T cells (Tconvs), limiting its in vivo application (14, 15). In contrast, we found that OX40L-JAG1–induced TCR-independent Treg proliferation to be selective because of the preferential/constitutive expression of their cognate receptors OX40 and Notch3 on Tregs over Tconvs. More importantly, soluble OX40L and JAG1 cotreatment induced selective proliferation of Tregs from NOD mice ex vivo, increased Tregs in vivo, and delayed the onset of diabetes, suggesting the potential utility of this approach to expand Tregs for treating type 1 diabetes (16). However, the signaling involved in TCR-dependent versus TCR-independent Treg proliferation remained poorly understood, and a better understanding of differential signaling, if it exists, might aid in selectively inhibiting TCR-dependent cell proliferation while permitting TCR-independent Treg proliferation. During TCR-dependent Treg expansion in vitro, repeated TCR stimulation can induce cell cycle–dependent recruitment of DNA methyltransferase (DNMT) 1, which facilitates methylation of the TSDR, leading to loss of Foxp3 expression in a subset of Tregs and gives rise to pathogenic ex-Foxp3 cells producing inflammatory cytokines (17). We speculated that the signaling required for Treg expansion and the epigenetic changes induced by OX40L-JAG1 might be different from that noted in TCR-dependent Treg proliferation. Additionally, the suitability of this approach to treat other autoimmune diseases and expand human Tregs remained to be determined.

In the current study, we showed that OX40L-JAG1 can induce proliferation of lineage-stable Tregs in vivo; TCR-dependent versus TCR-independent Treg proliferation were driven by distinct signaling pathways; OX40L-JAG1 treatment could prevent experimental autoimmune thyroiditis (EAT) in mice; and OX40L-JAG1–induced Treg expansion is conserved in humans.

Materials and Methods

Animals, human tissues, and Abs

C57BL/6J (stock no. 000664), NOD/ShiLtJ (stock no. 001976), OX40^{−/−} (stock no. 012838), Foxp3.eGFP (stock no. 018628), CBA/J (stock no. 000656), and NSG (NOD.Cg-*Prkdc*[scid] *Il2rg*[tm1Wjl]/SzJ; stock no. 005557) mice were purchased from The Jackson Laboratory. Breeding colonies were established and maintained in a pathogen-free facility of the biological resources laboratory of the University of Illinois at Chicago (Chicago, IL). All animal experiments were approved and performed in accordance with the guidelines set forth by the Animal Care and Use Committee at the University of Illinois at Chicago.

Normal pediatric thymus tissues (*n* = 16) were obtained through the Cooperative Human Tissue Network, Ohio State University, in accordance with the policies stated by the University of Illinois at Chicago Institutional Review Board. The Cooperative Human Tissue Network is funded by the National Cancer Institute, and other investigators may have received specimens from the same subjects.

Abs and reagents

Anti-mouse CD4 (clone no. GK1.5), anti-mouse CD8a (53.6.7), anti-mouse CD25 (PC61.5), anti-mouse/rat Foxp3 (FJK16S), anti-mouse Nur77 (12.14), anti-mouse CD134/OX40 (OX86), anti-human CD4 (RTA-T4), anti-human CD8a (SK1), anti-human FOXP3 (236A/E7 and PCH101), anti-human CD25 (BC96), anti-human CD134/OX40 (ACT35), anti-human CTLA4 (14D3), anti-human GITR (eBioAITR), anti-human TIGIT (MBSA43), anti-mouse/human Helios (22F6), anti-mouse CD11c (N418), anti-mouse CD39 (24DMS1), anti-mouse F4/80 (BM8), anti-mouse B220 (RA3-6B2), anti-mouse TIGIT (GIGD7), anti-mouse IFN-γ (XMG1.2), anti-mouse OX40 (OX86), anti-mouse GITR (DTA1), anti-mouse/RAT IL-17A (EBIO17B7), anti-mouse IL-4 (11B11), anti-mouse CTLA-4

(UC10-4B9), anti-mouse CCR4 (2G12), anti-human CD45 (HI30), and appropriate isotype control Abs were purchased from eBioscience and Thermo Fisher Scientific. Anti-Bcl2 (BCL/10C4), anti-human/mouse Ki67 (11F6), anti-mouse CD69 (H1.2F3), anti-mouse PD1 (29F.1A12), anti-mouse LAG-3 (C9B7W), anti-mouse Tim-3 (B8.2C12), and anti-human CD45RA (HI100) were purchased from BioLegend. CD4^{+}/CD4^{+}CD25^{+} EasySep T Cell Isolation kits were from StemCell Technologies. Mouse recombinant OX40L-Fc was provided by Dr. A. L. Epstein (Keck School of Medicine at University of Southern California, Los Angeles, CA). Mouse recombinant JAG1-Fc was produced from stable CHO(r) cells expressing soluble JAG1, as described previously (18). Human recombinant OX40L-Fc and JAG1-Fc were from Sino Biologicals. T cells were cultured in PRIME-XV T Cell Expansion XSFM Medium (Irvine Scientific). Purified porcine thyroglobulin was from Sigma-Aldrich. Mouse anti-CD3 (clone no. 2C11) and anti-CD28 (clone no. PV10) were purchased from BioXCell. Human and mouse recombinant IL-2 were from eBioscience and Thermo Fisher Scientific. Porcine thyroglobulin was from Sigma-Aldrich. Enzo Screen-Well Kinase Assay Library was provided by the High-Throughput Screening Core, Research Resources Center, University of Illinois at Chicago. Compounds PP1, R406, and AG-126 were from Selleckchem. Inhibitor of NF-κB inducible kinase (NIK) was generously gifted by Dr. N. Ghilradi, Genentech.

T cell proliferation assays and thymic organ culture

Spleen from 6- to 8-wk-old mice was excised, single-cell suspensions were prepared, and CD4^{+}/CD4^{+}CD25^{−}/CD4^{+}CD25^{+} T cells were isolated according to the manufacturer's (StemCell Technologies) protocol. Isolated cells were stained with CellTrace Violet (Life Technologies) and treated with IL-2 (25 U/ml), recombinant OX40L-Fc (5 μg/ml), JAG1-Fc (1 μg/ml), and anti-CD3/CD28 mAbs (2 μg/ml each) for the indicated durations. For kinase inhibition assays, cells were pretreated with inhibitors for 2 h and then stimulated with either OX40L-JAG1 or anti-CD3/CD28 for 4 d. Human thymuses were dissected into ∼2-mm[3] fragments and cultured over Matrigel (Corning) in 24-well transwell plates with PRIME-XV T Cell Expansion XSFM Medium in the presence of IL-2; human OX40L-Fc and JAG1-Fc were prepared and used, as described previously (19).

Flow cytometry and FACS analysis

Cells were washed with PBS containing 0.5% BSA, surface stained followed by fixation and permeabilization using Foxp3/Transcription Factor Staining Buffer Kit (Tonbo Biosciences), and stained with appropriate isotype controls and test Abs in the dark at 4˚C. Samples were analyzed using CyAn ADP Analyzer and CytoFLEX (Beckman and Coulter), and data were analyzed using Summit v4.3 and Kaluza v2.1 software (Beckman and Coulter). In some experiments, cell proliferation was measured by division index, calculated using FlowJo v10.6.1 (BD Biosciences). FACS sorting was performed using MoFlo Astrios Cell Sorter (Beckman and Coulter). Sort purity was >95%, as confirmed by postsort analysis.

Microarray and whole genome bisulfite sequencing analyses

For microarray analysis, Foxp3.GFP[+] Tregs were sorted from fresh, OX40L-JAG1, and anti-CD3/DC28 treated cultures. Total RNA was isolated from these cells using RNAeasy columns (Qiagen) converted into cDNA, and microarray analysis was performed in duplicate using the Affymetrix GeneChip Mouse Genome 430 2.0 Microarray at the Center for Genomics core facility at the University of Illinois at Chicago. Briefly, biotinylated cDNA was synthesized from total RNA using biotinylated dNTPs and allowed to hybridize with microarrays and scanned. Arrays passing quality control tests were further subjected to gene expression analysis after normalization with housekeeping gene controls. Data were analyzed using the R package software.

For whole genome bisulfite sequencing (WGBS), genomic DNA was isolated from sorted CD4^{+}CD25^{−} and CD4^{+}CD25^{+} T cells. Shotgun genomic libraries were prepared with the Hyper Library Construction Kit from Kapa Biosystems (Roche) and treated with the Lightning EZ Kit from Zymo Research. The libraries were quantitated by quantitative PCR and sequenced on one lane for 151 cycles from each end of the fragments on a NovaSeq 6000. Fastq files were generated and demultiplexed with the bcl2fastq v2.20 Conversion Software (Illumina). Reads were mapped to the reference genome in a bisulfite conversion–aware manner using Bismark. Apparent PCR duplicates were removed using deduplicate_bismark. Methylation status per read was obtained with bismark_methylation_extractor. Methylation percentage levels, plus counts of methylated and unmethylated bases, were then summarized per CpG. CpGs were further filtered to the subset with measurable

methylation levels (minimum 10× coverage) in all the samples of differential analysis. The lineage stability of Tregs was analyzed in terms of methylation percentage in Treg signature genes, such as *Foxp3, Il-2ra, Ctla4, Ikzf2,* and *Ikzf4.* Refer to National Center for Biotechnology Information Gene Expression Omnibus accession identifiers GSE136582 (https://www.ncbi.nlm.nih.gov/geo/query/acc.cgi?acc=GSE136582) and GSE130617 (https://www.ncbi.nlm.nih.gov/geo/query/acc.cgi?acc=GSE130617) for more information.

Western blot

$CD4^+CD25^+$ T cells (2×10^6 cells per milliliter) were treated with soluble OX40L, JAG1, and IL-2 or anti-CD3/D28, as described above. Cells were washed with PBS and lysed in Laemmli buffer (Bio-Rad). Proteins were resolved in 10% SDS-PAGE gels and transferred to PVDF Membranes (Bio-Rad), blocked with 5% skimmed milk, and incubated with primary anti-mouse TRAF1 (1:1000; Santacruz Biotechnologies), anti-mouse phospho p65 (Ser536) (1:500), and anti-mouse NF-κB2 p100/p52 Abs (1:500; Cell Signaling Technology). Blots were then washed, incubated with secondary anti-rabbit IgG-HRP, and developed using ECL Detection Kit (Pierce Scientific). Blots were stripped and reprobed with the anti-mouse β-actin–HRP Ab (1:5000; Santacruz Biotechnology) and anti-mouse p65 (1:1000; Cell Signaling Technology) and developed.

Animal experiments

Eight-week-old female NOD mice ($n = 6$ per group) were injected (i.p.) with recombinant OX40L (100 μg) and JAG1 (100 μg) once a week for three consecutive weeks. Age- and sex-matched control mice received PBS. On week 12, mice were sacrificed and analyzed for Treg numbers and suppressive phenotype. $CD4^+CD25^-$ Tconvs and $CD4^+CD25^+$ Tregs were sorted and subjected to WGBS, as described above.

For EAT induction, 6- to 8-wk-old female CBA/j mice were divided into three groups ($n = 6$ mice per group), namely 1) CFA control, 2) PBS vehicle control, and 3) OX40L-JAG1 (100 μg each). Mice were treated with PBS or OX40L-JAG1 on day 1, 7, and 14. On day 12, mice were immunized with CFA alone or CFA + porcine thyroglobulin (100 μg) emulsion s.c. to induce EAT (20, 21). A booster dose was given on day 26. On day 40, mice were euthanized, and spleen, draining lymph nodes (dLNs) of thyroid and neck region, and thyroid tissue were harvested. Serum samples were analyzed for anti–porcine thyroglobulin IgG Abs by ELISA. dLN cells were stimulated with thyroglobulin Ag (20 μg/ml) in the presence of PMA-ionomycin for 6 h and protein transport inhibitor mixture (eBioscience) for final 2 h and analyzed for $CD4^+Foxp3^-IFN-\gamma^+$, $IL-4^+$, and $IL-17^+$ Teffs by flow cytometry.

Thyroid tissues from CFA-, PBS-, and OX40L-JAG1–treated mice were excised and fixed in 10% formalin and processed for H&E staining. Thyroiditis scoring was done as described previously (22). Scoring was done on a scale of 1–5 with reference to the extent of lymphocyte infiltration in blinded fashion by two individuals: 1) infiltration of at least 125 cells in one or several foci, 2) 10–20 foci of cellular infiltration with up to 25% of the gland, 3) infiltration of up to 25–50%, 4) >50% destruction of the gland, and 5) near-complete destruction of the gland.

Twenty-two–week–old female NSG mice engrafted with human CD34 precursors at 4 wk of age at The Jackson Laboratory were used to study the effect of OX40L-JAG1 treatment on human Tregs in vivo. Engraftment efficiency was checked by quantifying human $CD45^+$ cells in the peripheral blood before treatment. Distribution frequency of human $CD45^+$ cells ranged from 38.6 to 65.0%. Mice were divided randomly ($n = 4$) and treated with PBS or human OX40L and JAG1 (100 μg each) three times at 5-d intervals. Mice were sacrificed a week after the final treatment. Spleen and liver were collected, and single-cell suspensions were prepared and analyzed for increased human Tregs by flow cytometry, as described above.

In vitro suppression assays

Suppression assays were performed by coculturing anti-CD3 (0.5 μg/ml)-stimulated $CD4^+CD25^-$ (Teffs) and $CD4^+CD25^+$ (Tregs) in the presence of thyroglobulin (20 μg/ml)-loaded APCs at 1:0, 1:1, 1:2, 1:4, and 1:8 Teff/Treg ratios for 3 d. The extent of suppression was measured using the division index of Teffs in no Treg control versus Treg cocultures.

Statistical analysis

Statistical analyses were performed using Prism GraphPad (v6.0). Data were expressed as mean ± SEM of multiple experiments. Student *t* test was used to compare two groups, whereas ANOVA with Tukey multiple comparisons was used to compare more than two groups. A *p* value <0.05 was considered significant.

Results

OX40L-JAG1–induced selective Treg proliferation is not blocked by the inhibition of proximal TCR signal initiating Src family kinase

Previous studies from our laboratory have shown that OX40L-JAG1 cosignaling can induce selective expansion of $Foxp3^+$Tregs, but not $Foxp3^-$Teffs, independent of TCR stimulation (13, 16). Therefore, we investigated as to why Tregs proliferated independent of TCR stimulation whereas Tconvs did not. We performed differential gene expression profiling of $Foxp3^+$ Tregs and $Foxp3^-$ Tconvs sorted from Foxp3.GFP reporter mice and found that Tregs had higher expression levels of T cell activation–related genes like *CD25, OX40, GITR, 4-1BB, TNFR2, CD69, Nur77, IL-2Ra,* and *IL-2Rb* compared with Tconvs (Supplemental Fig. 1A). Moreover, Tregs had increased the $CD44^{hi}$ $CD62^{low}$ activated population and decreased the $CD44^{low}$ $CD62L^{hi}$ naive population compared with Tconvs under resting conditions (Supplemental Fig. 1B, 1C). These results suggested a lower activation threshold required for Treg proliferation compared with Tconvs, which can be achieved without TCR stimulation.

Total $CD4^+$ T cells were pretreated with a library of kinase (e.g., CDK, CKI and II, EGFR, GSK, IKK, insulin receptor, JAK, JNK, MAPK, MEK, PI3-kinase, AKT, mTOR, PDGFR, PKA, PKC, and Src family, etc.) inhibitors and stimulated with anti-CD3/CD28 mAbs or soluble OX40L-JAG1. Treg and Teff proliferation was assayed by CellTrace Violet dilution assay. Inhibitors causing >50% cell death were eliminated from analysis. Proliferation index was calculated as the ratio between proliferating/resting Tregs. Inhibitors causing 50% reduction in the proliferation index with respect to the proliferation index of no inhibitors control in both treatments are shown in Supplemental Fig. 1D. Inhibitors of MEK (U-0126), p38 MAPK (SB-203580 and SB-202190), PKA-PKG-MLCK-PKC (H7-2HCl), PDGFRK (tyrphostin 9), GSK-3-β (Indirubin-3′-monoxime), IKK2 (sc-514), PI3K (LY 294002 and wortmannin), Akt (BML-257), mTOR (rapamycin), and CDK (Roscovitine) effectively inhibited both anti-CD3/CD28 mAbs and OX40L-JAG1–induced Treg proliferation. Inhibitors of Src family kinase (PP1 and PP2), JAK-2 (AG-490), EGFRK (Erbstatin analogue), and cRAF (GW 5074) specifically inhibited anti-CD3/CD28-induced Treg and Teff proliferation but not OX40L-JAG1–induced Treg proliferation. Thus, OX40L-JAG1–induced TCR-independent Treg proliferation was not blocked by the inhibitors of proximal TCR signaling kinase, such as Src family kinase, but both anti-CD3/CD28– and OX40L-JAG1–induced Treg proliferation was inhibited by inhibitors of downstream signaling pathways, like PKC, PI3-K-AKT-mTOR, and MEK pathways (Supplemental Fig. 1D).

During TCR-mediated T cell proliferation, recognition of peptide-MHC complex by TCRs leads to activation of Lck (a member of Src family kinases), which phosphorylates ITAMs of CD3 and ζ-chain, leading to the recruitment and phosphorylation of Syk family kinase (ZAP70). Activated ZAP70 then propagates signaling downstream of TCR (23). Although Src and Syk family kinases predominantly mediate TCR-dependent T cell proliferation, their plausible role in TCR-independent T cell proliferation had not been ruled out. Furthermore, to avoid interference from IL-2 produced by Teffs in total CD4 T cell culture that might boost Treg proliferation/differentiation (24), we sorted $CD4^+CD25^-$ Tconvs and $CD4^+CD25^+$ Tregs and pretreated them with the inhibitors of Src kinase (PP1), SYK (R406), and IRAK (AG-126) and stimulated them with IL-2

alone or anti-CD3/CD28 or OX40L-JAG1 with IL-2 and measured Teff/Treg proliferation using the cell division index. IL-2 and OX40L-JAG1 did not induce Teff proliferation, whereas anti-CD3/CD28 treatment induced significant proliferation of both Teffs and Tregs as shown by a higher cell division index. Anti-CD3/CD28–induced Teff proliferation was significantly inhibited by Src and Syk kinase inhibitors, as evidenced by a significant reduction in cell division index. IL-2 induced basal proliferation of Tregs, which was further enhanced by the addition of OX40L-JAG1. Whereas anti-CD3/CD28-induced proliferation of Tregs was suppressed by the inhibitors of Src and Syk kinases (Fig. 1A, 1B), they had little or no effect on either IL-2 alone or OX40L-JAG1–induced Treg proliferation.

To further ascertain the differential role of Src kinase signaling in TCR-dependent versus -independent T cell activation and proliferation, we stimulated CD4^{+} T cells with anti-CD3/CD28 and OX40L-JAG1 in the presence/absence of Src kinase inhibitor PP1 and analyzed the expression of T cell activation markers, such as CD69 and CD25 in Foxp3^{−} Teffs and Foxp3^{+} Tregs (Fig. 1C–E). Increases in the expression of CD69 and CD25 after anti-CD3/CD28 stimulation were significantly suppressed upon PP1 treatment in both Teffs and Tregs. In contrast, we observed a significant increase in CD69 and CD25 expression in Tregs upon OX40L-JAG1 treatment both in the presence or absence of PP1. However, there was no increase in the levels of expression of CD69 and CD25 in Teffs upon IL-2 and OX40L-JAG1 treatment, and levels remained unaltered in the presence of PP1 (Fig. 1C–E).

TCR-independent Treg proliferation is induced via OX40-TRAF1–mediated noncanonical NF-κB signaling

Unlike the molecular mechanisms of TCR-dependent Treg proliferation, which are well documented, those of TCR-independent Treg proliferation are not completely known. Earlier, we had shown the involvement of canonical NF-κB signaling and AKT-mTOR
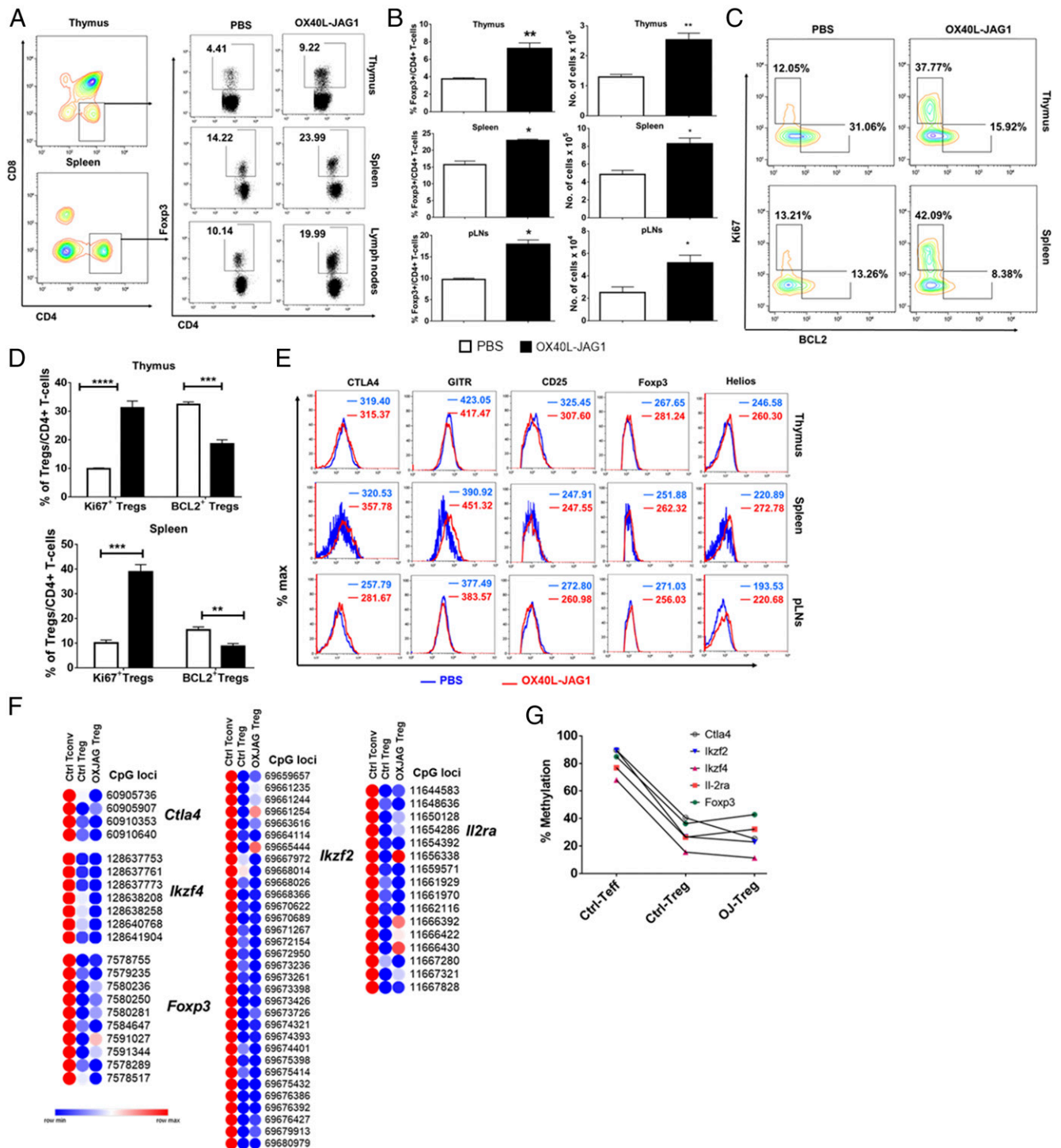
signaling in this Treg proliferation (16, 25). However, these pathways are not specific to OX40L-JAG1–induced proliferation as they can also mediate TCR-dependent Treg proliferation (Supplemental Fig. 1D). To determine the specific signaling pathway mediating OX40L-JAG1–induced TCR-independent Treg proliferation, but not TCR-dependent Treg proliferation, we analyzed the gene expression profile of fresh, anti-CD3/CD28–, and OX40L-JAG1–expanded Foxp3.GFP Tregs. In silico pathway analysis using Metacore software (Thomson Reuters) identified differential expression of a gene cluster related to noncanonical NF-κB activation involving *TRAF1, TRAF5, RelB*, and *NF-kB2* genes in OX40L-JAG1–expanded Tregs relative to anti-CD3/CD28-expanded and control Tregs (Fig. 2A). Genes involved in canonical NF-κB signaling such as RelA and *NF-kb1* were upregulated in Tregs expanded by both OX40L-JAG1 and anti-CD3/CD28 stimulation compared with control Tregs. We also found specific upregulation of *Dnmt1* in anti-CD3/CD28–expanded Tregs compared with control and OX40L-JAG1–expanded Tregs (Fig. 2A).

Interestingly, NIK (NF-κB inducing kinase of noncanonical NF-κB signaling) inhibitor selectively blocked OX40L-JAG1–induced, but not IL-2– or anti-CD3/CD28-induced, Treg proliferation (Fig. 2B, 2C). Further, we found increased TRAF1 and p100 to p52 processing in OX40L-JAG1–treated Tregs compared with anti-CD3/CD28-treated Tregs, whereas p65 phosphorylation was increased in both OX40L-JAG1– and anti-CD3/CD28-treated Tregs, which is in line with our gene expression profiling results (Fig. 2D). Next, we analyzed the effects of treatment with either OX40L or JAG1 on noncanonical NF-κB activation. Whereas OX40L activated p100 to p52 processing, JAG1 failed to show a synergistic effect on OX40L-induced noncanonical NF-κB signaling (Fig. 2E). Furthermore, TRAF1 and p100 to p52 processing were decreased in OX40^{−/−} Tregs compared with wild-type Tregs in the presence/absence of OX40L stimulation (Fig. 2F). Taken together, these results showed OX40L-induced noncanonical
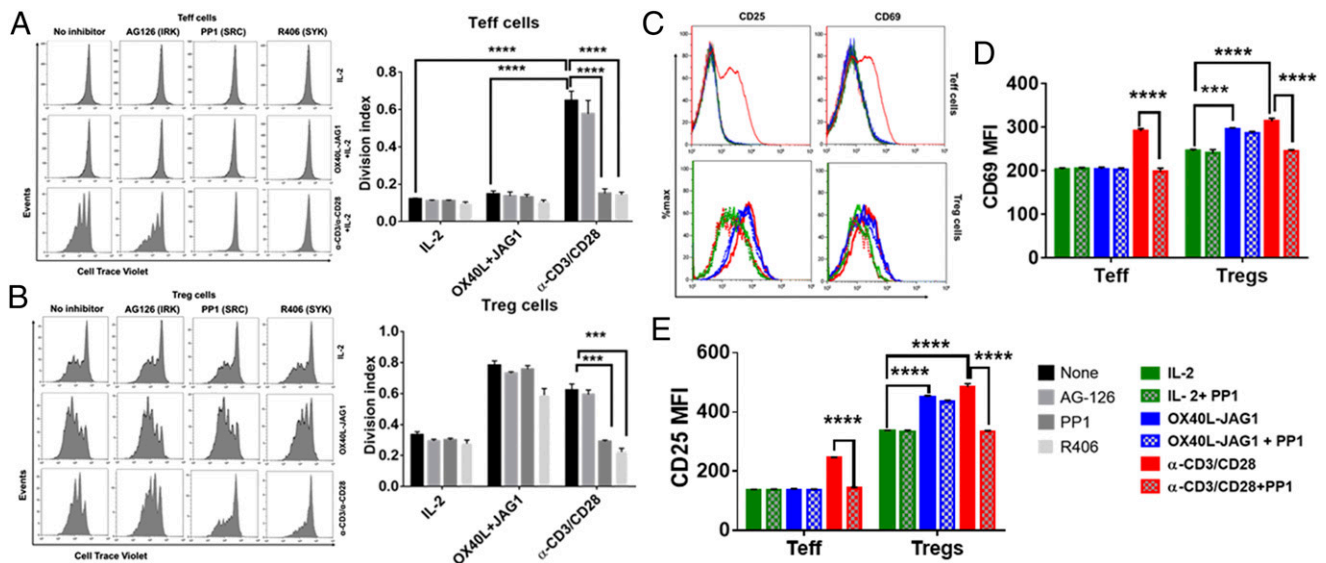
FIGURE 1. (**A** and **B**) CD4^{+}CD25^{−} Tconvs (A) and CD4^{+}CD25^{+} Tregs (B) were pretreated with indicated kinase inhibitors (10 μM/ml) for 2 h and cotreated with IL-2 (25 U/ml) and OX40L (5 μg/ml) + JAG1 (1 μg/ml) and anti-CD3 + anti-CD28 mAbs in the presence of IL-2 for 4 d. Cell proliferation was measured by CellTrace Violet dilution assay. Bar graphs show division index calculated from CellTrace Violet dilution in each culture condition (values represent mean ± SEM; $n = 3$). ****$p < 0.001$, ***$p < 0.05$. (**C**) Overlay histograms show CD69 and CD25 expression in gated CD4^{+}Foxp3^{−} Teffs (top panel) and CD4^{+}Foxp3^{+} Tregs (bottom panel) from the above experiments. Bar graphs show mean fluorescence intensity values of CD69 (**D**) and CD25 expression (**E**) in Teffs and Tregs summarized from (C). Values are expressed as mean ± SEM ($n = 3$ independent experiments). ***$p < 0.005$, ****$p < 0.001$.

FIGURE 2. (**A**) CD4^{+} T cells from Foxp3.GFP mice were treated with OX40L-JAG1 or anti-CD3/CD28 for 3 d. CD4^{+}Foxp3^{−}GFP^{−} Teffs and CD4^{+}Foxp3^{+}GFP^{+} Tregs were sorted and subjected to microarray analysis. Unstimulated fresh Teffs and Tregs were used as a control. Heat map shows differential mRNA expression of TRAFs, NF-κB, and DNMT signaling-related genes between control, OX40L-JAG1–, and anti-CD3/CD28-treated Tregs. (**B**) CD4^{+}CD25^{−} Tconvs and CD4^{+}CD25^{+} Tregs were pretreated with indicated NIK inhibitor (10 μM/ml) for 2 h and cotreated with IL-2 (25 U/ml), OX40L (5 μg/ml) + JAG1 (1 μg/ml), and anti-CD3 + anti-CD28 mAbs in the presence of IL-2 for 4 d. Cell proliferation was measured by CellTrace Violet dilution assay. (**C**) Bar graphs show division index calculated from CellTrace Violet dilution in each culture conditions (values represent mean ± SEM; $n = 3$). ****$p < 0.001$. (**D**) Western blots show TRAF1 expression, p100 to p52 processing, and total and phospho p65 levels in OX40L-JAG1–treated Tregs compared with fresh and anti-CD3/CD28–treated Tregs after 24 h. (**E**) Western blots show p100 to p52 processing in Tregs treated with IL-2 alone, JAG1 alone, OX40L alone, and OX40L + JAG1 + IL-2. (**F**) Western blots show TRAF1 and p100 to p52 processing in wild-type and OX40^{−/−} Tregs treated with or without OX40L.

NF-κB signaling as a key signaling mechanism differentially driving TCR-independent Treg proliferation.

OX40L-JAG1 treatment induces Treg proliferation in vivo and expands lineage-stable Tregs in autoimmune-prone NOD mice

Earlier, we had shown that OX40L-JAG1 treatment of prediabetic NOD (10- to 12-wk-old) mice increased Tregs in the periphery and delayed the onset of autoimmune diabetes (16). However, we did not determine if it involved increased thymic output or increased Treg survival/proliferation. Therefore, we treated prediabetic female NOD mice with OX40L-JAG1 and found significantly increased Treg frequency and numbers in the thymus (**$p < 0.01$), spleen (*$p < 0.05$), and peripheral lymph nodes (*$p < 0.05$) (Fig. 3A, 3B). We also analyzed the expression of proliferation marker Ki67 and prosurvival factor BCL2, which arrests cell cycle progression (26, 27). There was

a significant increase in Ki67^{+}BCL2^{−}Foxp3^{+} proliferating Tregs (****$p < 0.001$ in thymus and ***$p < 0.005$ in spleen) and a significant reduction in Ki67^{−}BCL2^{+}Foxp3^{+} resting Tregs (***$p < 0.01$ in thymus and **$p < 0.005$ in spleen) in OX40L-JAG1–treated mice compared with PBS-treated mice (Fig. 3C, 3D). These results indicated that it is the increased Treg proliferation, and not increased survival, that contributed to the increase in Tregs. To further confirm that OX40L-JAG1 treatment significantly increased matured thymic Tregs and Treg precursors, we analyzed CD4^{+}CD25^{+}Foxp3^{−}/CD4^{+}CD25^{−}Foxp3^{low} Treg precursors and CD4^{+}CD25^{+}Foxp3^{+} Tregs in the thymus and found a significant increase in CD4^{+}CD25^{−}Foxp3^{low} Treg precursors and CD4^{+}CD25^{+}Foxp3^{+} matured Tregs (****$p < 0.001$) with no significant increase in CD4^{+}CD25^{+}Foxp3^{−} Treg precursors (Supplemental Fig. 2A). Further, the increased thymic Tregs could contribute to increased peripheral Treg numbers.

FIGURE 3. (**A**) Six- to eight-week-old female NOD mice were injected with PBS or soluble OX40L and JAG1 (100 μg each) once a week for three consecutive weeks, and percentages of CD4$^+$Foxp3$^+$ Tregs were analyzed in the thymus, spleen, and peripheral lymph nodes. (**B**) Bar graphs show frequency of and number of Tregs (values represent mean ± SEM, $n = 6$). *$p < 0.05$, **$p < 0.01$. (**C**) CD4$^+$Foxp3$^+$ from the thymus and spleen were gated, and contour plots show Ki67$^+$BCL2$^-$ (proliferating) and Ki67$^-$BCL2$^+$ (resting) cells. (**D**) Bar graphs summarize frequencies of Ki67$^+$BCL2$^-$ (proliferating) and Ki67$^-$BCL2$^+$ (resting) Tregs in the thymus and spleen calculated from (C). Values represent mean ± SEM, $n = 6$. **$p < 0.01$, ***$p < 0.005$, ****$p < 0.001$. (**E**) Overlay histograms show the expression levels of Treg signature markers CTLA4, GITR, CD25, Foxp3, and Helios in CD4$^+$Foxp3$^+$ cells in the thymus, spleen, and pancreatic lymph nodes of PBS- (blue) versus OX40L- (red) treated mice. (**F**) Heat maps show methylation index of individual CpG islands between control and OX40l-JAG1–treated Tregs compared with control Teffs. (**G**) Methylation percentage levels in the promoter and intronic regions of Treg signature genes *Ctla4, Ikzf4, Ikzf2, Il-2ra,* and *Foxp3* in sorted splenic CD4$^+$CD25$^+$ Tregs and CD4$^+$CD25$^-$ Teffs from PBS- and OX40L-JAG1–treated NOD mice as analyzed by WGBS.

Next, we analyzed peripheral Treg expansion in the absence of continuous thymic Treg output in thymectomized NOD mice and observed increased Tregs in the spleen of thymectomized

mice upon OX40L-JAG1 treatment compared with control mice (*$p < 0.05$), indicating Treg expansion in the periphery (Supplemental Fig. 2B). These data indicated that increased

thymic Treg differentiation and proliferation and peripheral Treg proliferation might contribute to increased Treg numbers.

Next, we investigated the lineage stability of OX40L-JAG1–expanded Tregs and found sustained expression of Treg lineage stability markers CD25, CTLA4, Helios, and GITR in CD4$^+$Foxp3$^+$ cells from the thymus, spleen, and peripheral lymph nodes of control versus OX40L-JAG1–treated mice (Fig. 3E). Furthermore, the epigenetic stability of Treg lineage was evaluated by analyzing the methylation levels of the nTreg signature genes in sorted CD4$^+$CD25$^+$ Tregs and CD4$^+$CD25$^-$ Tconvs from PBS- and OX40L-JAG1–treated mice by WGBS. Treg-specific de/hypomethylated regions were selected by comparing methylation levels between CD4$^+$CD25$^+$ Tregs (20–40%) and CD4$^+$CD25$^-$ Tconvs (70–90%) from control mice. As shown in Fig. 3F and 3G, we observed minimal differences in the degree of methylation in the relevant CpG islands between control and OX40L-JAG1–expanded Tregs, indicating that OX40L-JAG1 stimulation did not lead to hypermethylation of the relevant CpG islands and thus might have contributed to their lineage stability.

OX40L-JAG1 treatment expands functional Tregs and ameliorates EAT

We examined whether OX40L-JAG1 cotreatment can expand functionally suppressive Tregs and prevent EAT in CBA/j mice, which is a highly susceptible strain for EAT induction (28). First, we treated 6-wk-old CBA/j mice with soluble OX40L and JAG1 once a week for 2 wk and immunized them with porcine thyroglobulin emulsified in CFA. An additional (third) OX40L-JAG1 treatment was given 2 d after immunization. Mice received booster immunization 14 d after the first immunization. Mice were monitored for thyroiditis development 14 d after the booster dose. A subset of mice was sacrificed after final OX40L-JAG1 treatment to determine the suppressive phenotype and functionality of Tregs. We observed significantly increased Tregs in the thymus (***$p < 0.001$), spleen (***$p < 0.001$), and dLNs (**$p < 0.01$) of OX40L-JAG1–treated mice (Fig. 4A), with significantly increased frequencies of CTLA4$^+$Foxp3$^+$ and TIGIT$^+$ Foxp3$^+$ Tregs in the spleen (***$p < 0.005$) and dLNs (*$p < 0.05$ [CTLA4] and ***$p < 0.005$ [TIGIT]) (Fig. 4B). In addition, increased TIM3$^+$Foxp3$^+$ and PD1$^+$Foxp3$^+$Tregs were observed in the spleen but not dLNs (Fig. 4B). Additionally, expression levels of CTLA4, TIGIT, and TIM3 were also significantly increased in OX40L-JAG1–expanded Tregs in the spleen and lymph nodes (Fig. 4C). Increased CTLA4$^+$/TIGIT$^+$ Foxp3$^+$ Tregs and CTLA4/TIGIT expression per se were observed in OX40L-JAG1–treated mice compared with control mice (Fig. 4D). We did not find any difference in the total CD4$^+$ T cells, CD8$^+$ T cells, B220$^+$ B cells, F4/80$^+$CD11c$^-$ macrophages, and F4/80$^-$CD11c$^+$ dendritic cells in the spleen and lymph nodes of PBS- versus OX40L-JAG1–treated mice (Supplemental Fig. 3A), indicating the major effect of the treatment was on the Treg compartment. Furthermore, we observed higher levels of suppression of Teff proliferation when cocultured with Tregs from OX40L-JAG1–treated mice compared with PBS-treated mice (Fig. 4E–G), which is in line with enhanced expression of suppressive markers in these Tregs. Treg suppressive functions were generally higher against OX40L-JAG1–treated Teffs, indicating that these Teffs were more sensitive to Treg suppression.

As shown in Fig. 5A and 5B, we noticed splenomegaly and lymphadenopathy in thyroglobulin-immunized control mice compared with CFA control and OX40L-JAG1–treated mice. Histopathology and thyroiditis scores showed significantly

increased lymphocyte infiltration in thyroglobulin-immunized and PBS- (***$p < 0.005$) treated mice compared with CFA alone–treated mice. In contrast, significantly reduced (**$p < 0.01$) lymphocytic infiltration with more intact thyroid follicles were seen in thyroglobulin-immunized OX40L-JAG1–treated mice compared with PBS-treated mice (Fig. 5C, 5D). Reduced antithyroglobulin Ab titers were also seen in OX40L-JAG1–treated mice (Fig. 5E). Furthermore, intracellular cytokine staining showed increased IL-4$^+$ Th2 cells in the dLNs in PBS-treated mice compared with OX40L-JAG1–treated mice. Upon in vitro stimulation, proinflammatory IFN-γ, IL-4, and IL-17 cytokine expressions were significantly increased in PBS-treated mice, whereas IL-4, but not IFN-γ and IL-17, expression was significantly reduced in OX40L-JAG1–treated mice (Fig. 5F, 5G).

Human OX40L-JAG1 treatment induces TCR-independent proliferation of human Tregs

Next, we examined whether human OX40L-JAG1 can expand human Tregs. First, we analyzed the expression levels of OX40 in CD4$^+$Foxp3$^+$ Tregs and CD4$^+$Foxp3$^-$ Tconvs from human and murine PBMCs, spleen, and thymus. Interestingly, we observed very low levels of OX40 expression in Tregs from the PBMCs compared with those from spleen and thymus. Similarly, Tconvs had very low levels of OX40 expression (Supplemental Fig. 4). Furthermore, we observed a significant increase (**$p < 0.01$) in human CD4$^+$CD25$^+$FOXP3$^+$ Tregs in OX40L-treated human thymic organ cultures compared with IL-2 alone–treated cultures. Although there was considerable increase in Tregs in JAG1 + IL-2–treated cultures, it was not significantly different from IL-2 alone. OX40L + JAG1–treated cultures showed the highest increase in Tregs (***$p < 0.005$) (Fig. 6A, 6B). Next, we treated thymocytes devoid of APCs with IL-2 alone or OX40L + JAG1 + IL-2 without TCR stimulation for 5 d and measured Treg proliferation. Although we found a significant increase in proliferating Tregs upon OX40L-JAG1 treatment compared with IL-2 control, we failed to find a significant increase in the proliferation of Foxp3$^-$ Tconvs (Fig. 6C, 6D).

Unlike murine Tregs in which Foxp3 expression is strictly confined to Tregs and accepted as a lineage-specific marker, transient expression of FOXP3 has been noted in nonregulatory activated Teffs lacking suppressive functions in humans (29, 30). Therefore, we analyzed the proportions of CD45RA$^-$Foxp3^{hi} (effector Tregs), CD45RA$^+$Foxp3^{low} (naive Tregs), and CD45RA$^-$Foxp3^{low} (effector-like T cells) and noted a significant increase in CD45RA$^-$Foxp3^{hi} effector Tregs and not in CD45RA$^-$Foxp3^{low} effector-like T cells upon OX40L-JAG1 treatment compared with IL-2 control (Fig. 6E). Furthermore, OX40L-JAG1–expanded Tregs had comparable levels of Treg markers, such as CTLA4, CD39, Helios, and TIGIT compared with IL-2 control Tregs (Fig. 6F), indicative of their ability to maintain suppressive phenotype. We tested the functional competency of OX40L-JAG1–expanded CD4$^+$CD25^{hi} Tregs by coculturing them with autologous CD4$^+$CD25$^-$ Tconvs and observed comparable suppressive function between fresh versus OX40L-JAG1–expanded Tregs (Fig. 6G, 6H).

Finally, we tested the ability of OX40L-JAG1 treatment to expand human Tregs in vivo using the humanized NSG mice engrafted with CD34 precursors. We did not observe any signs of graft-versus-host disease, such as weight loss/lethargy, in control or OX40L-JAG1–treated mice. Although the frequency of Foxp3^{hi} Tregs in human CD45$^+$CD4$^+$ T cells in the spleen was not significantly different from that in control mice, there was a significant increase in Foxp3^{hi} Tregs in the liver of treated mice (Fig. 6I). We found a significant increase within the
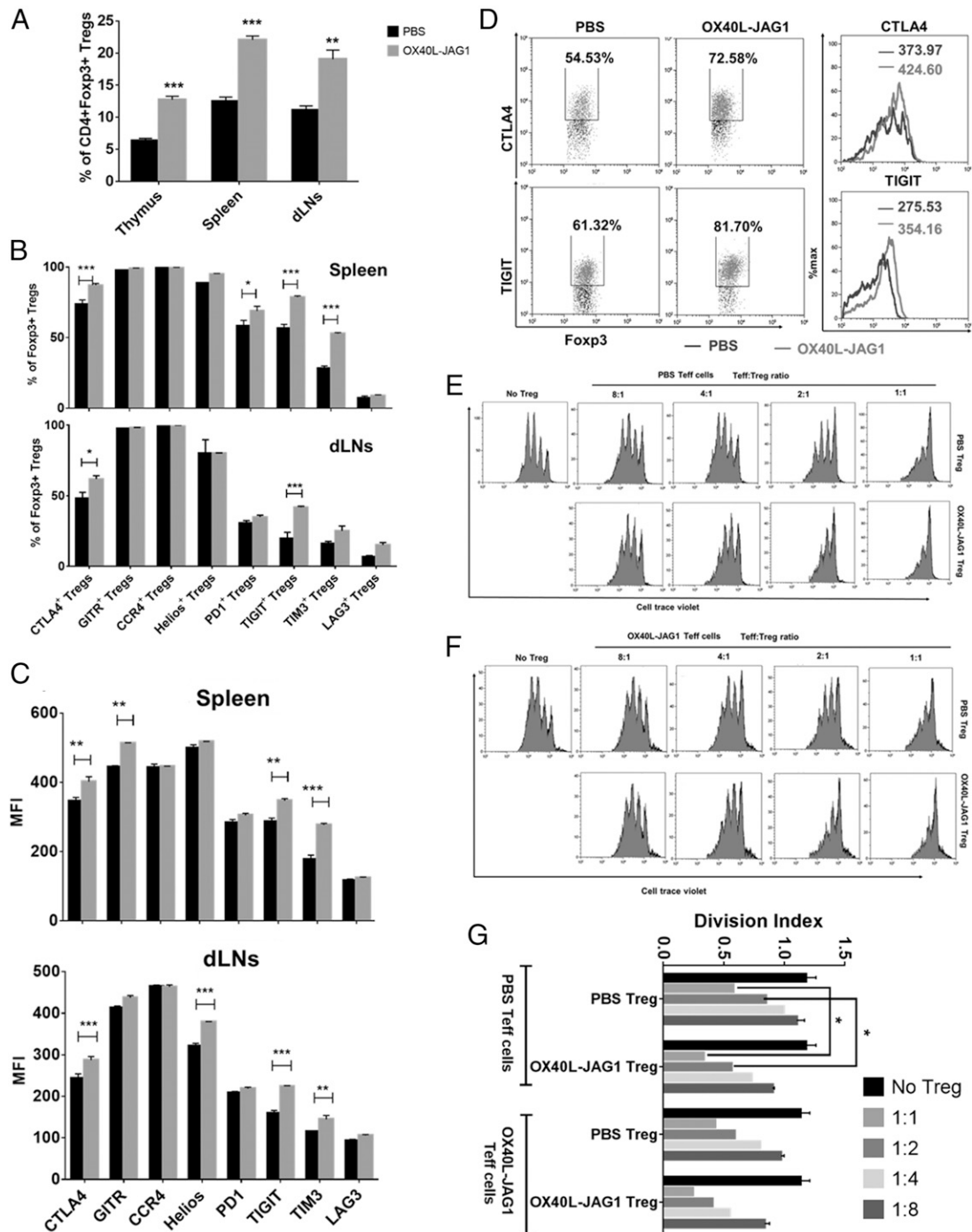
FIGURE 4. (**A**) Six- to eight-week-old female CBA/j mice were injected with PBS or soluble OX40L and JAG1 (100 μg each) and immunized with porcine thyroglobulin Ag emulsified with CFA. A subset of mice from PBS/OX40L-JAG1–treated mice were sacrificed immediately after first immunization, and last OX40L-JAG1 treatment is as described in *Materials and Methods*. Percentages of CD4^{+}Foxp3^{+} Tregs were analyzed in the thymus, spleen, and peripheral lymph nodes. Values represent mean ± SEM, $n = 6$. **$p < 0.01$, ***$p < 0.005$ versus PBS. (**B**) Frequencies of CTLA4^{+}, GITR[+], CCR4^{+}, Helios[+], PD1^{+}, TIGIT[+], TIM3^{+}, and LAG3^{+} Tregs in the spleen (top panel) and dLNs (bottom panel) were analyzed by flow cytometry. Values represent mean ± SEM, $n = 6$, *$p < 0.05$, ***$p < 0.005$ versus PBS. (**C**) Mean fluorescence intensity values of the above-mentioned suppressive markers are summarized. Values represent mean ± SEM, $n = 6$. **$p < 0.01$, ***$p < 0.005$ versus PBS. (**D**) Representative dot plots and overlay histograms show increased CTLA4^{+}/TIGIT^{+} Foxp3^{+} Tregs and CTLA4/TIGIT expression per se in OX40L-JAG1–treated mice. (**E** and **F**) PBS- and OX40L-JAG1–expanded CD4^{+}CD25^{+} Tregs from CBA/j mice were cocultured with CellTrace Violet–labeled CD4^{+}CD25^{−} Teffs from PBS- and OX40L-JAG1–treated mice in depicted combinations at indicated ratios and stimulated with anti-CD3 in the presence of thyroglobulin Ag (20 μg/ml)-loaded APCs for 3 d. The extent of Teff proliferation was measured by CellTrace Violet dilution assay. (**G**) Bar graphs show division index of Teffs calculated from each culture conditions (values represent mean ± SEM, $n = 3$). *$p < 0.05$.

CD45RA^{−}Foxp3^{hi} effector Treg subset in OX40L-JAG1–expanded Tregs (Fig. 6J) without loss of expression of suppressive markers CTLA4 and TIGIT (Fig. 6K).

Discussion

Positive selection of Tregs in the thymus requires higher TCR signal strength, which enables those cells to preferentially overexpress
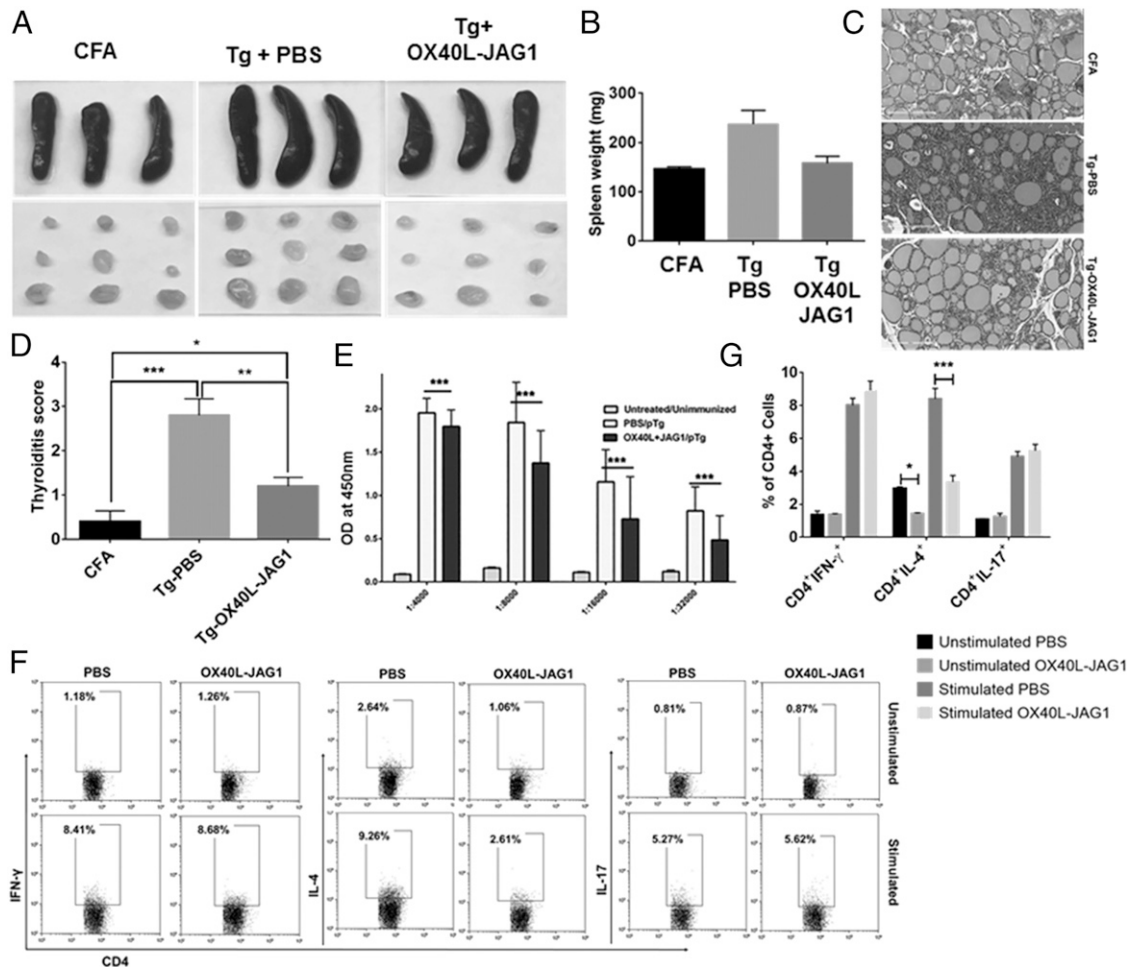
FIGURE 5. (**A**) All mice from thyroiditis experiments were sacrificed at the end of the experiment 14 d after the second immunization. Images of the spleen and dLNs are shown. (**B**) Bar graph summarizing spleen weights. (**C**) H&E staining analysis of thyroid sections (original magnification ×20) from CFA control, thyroglobulin-immunized, and PBS-treated or OX40L-JAG1 mice (*n* = 6). (**D**) Thyroiditis scoring was done as described in *Materials and Methods*. Values represent mean ± SEM, *n* = 6. *$p < 0.05$, **$p < 0.01$, ***$p < 0.005$. (**E**) Serum antithyroglobulin levels were measured by ELISA, and bar graph shows absorbance at 450 nm measured at different dilutions (values represent mean ± SEM, *n* = 6, ***$p < 0.005$). (**F**) Representative dot plots showing frequency of CD4$^+$Foxp3$^-$IFN-γ$^+$ Th1, CD4$^+$Foxp3$^-$IL-4$^+$ Th2, and CD4$^+$Foxp3$^-$IL-17$^+$ Th17 cells in the dLN cells before and after stimulation with PMA/ionomycin. (**G**) Bar graph summarizing results of (F) (values represent mean ± SEM, *n* = 6). *$p < 0.05$, ***$p < 0.005$ versus PBS.

T cell activation and costimulatory/coinhibitory receptors (such as CD25, ICOS, GITR, OX40, 4-1BB, CTLA4, PD-1, and TIGIT) relative to Tconvs, and they require TCR activation to gain expression of these receptors (31). This allows cosignaling receptors to selectively modulate Treg proliferation and function and thereby contribute significantly to Treg homeostasis and immune tolerance. In this study, we show that stimulation of OX40 and Notch3 receptors that are preferentially overexpressed on Tregs can lead to selective activation and proliferation of Tregs without concomitant expansion of Tconvs in T cell cultures in the absence of TCR stimulation. Earlier, studies had shown that a sharp TCR signaling threshold is obligatory for T cell proliferation (32). Although TCR signaling is activated shortly after TCR engagement, T cell proliferation is observed days later because of the time required for the propagation of progressive events to reach the threshold needed for proliferation. After reaching the threshold, T cells can proliferate even in the absence of TCR signaling, as evidenced by ZAP70 kinase-independent proliferation of T cells (32). It is possible that Tregs might have attained higher activation threshold than Tconvs during their thymic selection, which renders them susceptible to TCR-independent proliferation when stimulated through coactivation receptors,

such as OX40. Furthermore, inhibitors of proximal TCR signaling kinase, such as Src family kinase (PP1), blocked anti-CD3/CD28-induced TCR-dependent Tconv activation as evidenced by reduced CD69 and CD25 expression and proliferation, as well. Tregs, because of their selection against higher TCR signal strength, expressed higher levels of CD69 and CD25 relative to Tconvs under resting state, which was further increased upon TCR/OX40L-JAG1 stimulation. More importantly, TCR-dependent, but not TCR-independent, upregulation of CD69 and CD25 expression in Tregs was inhibited by PP1. These results suggest two key interpretations: 1) even TCR-independent stimulation through coactivation receptors like OX40/Notch3 can upregulate CD69 and CD25 expression in Tregs and 2) PP1 is a selective inhibitor of TCR-mediated T cell activation and proliferation, which does not inhibit TCR-independent activation/proliferation of Treg-induced upon OX40L-JAG1 treatment. These results suggested that Tregs differ from Tconvs in terms of their activation state and signaling requirement for proliferation and can be induced to proliferate with OX40L-JAG1 treatment in the absence of TCR stimulation.

We found a significant increase in Ki67$^+$BCl2$^-$ proliferating Tregs with a concomitant decrease in Ki67$^-$BCL2$^+$ resting Tregs
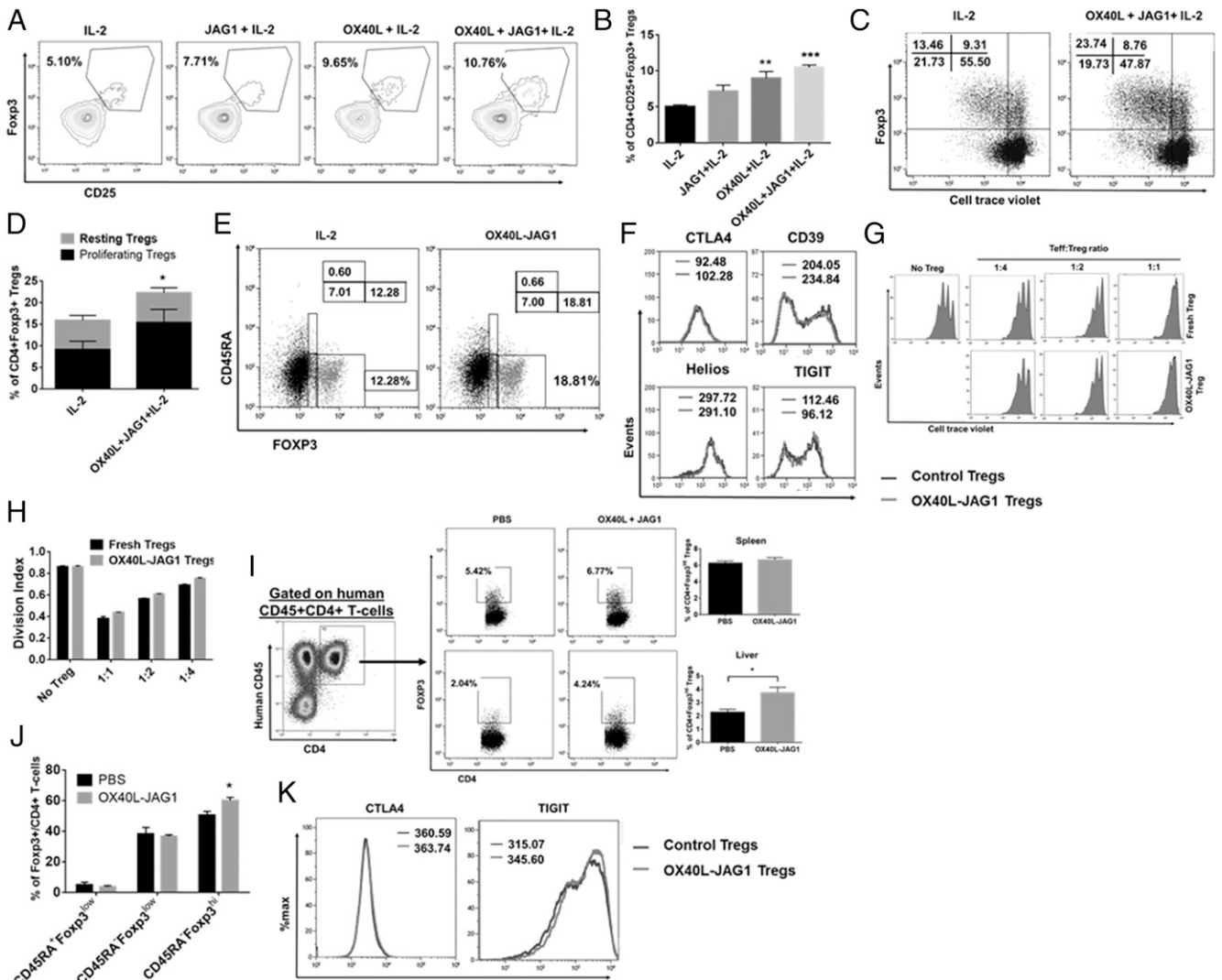
FIGURE 6. (**A**) Human thymic fragments were cultured in three-dimensional thymic organ cultures with human IL-2 (50 U/ml) or human JAG1-Fc (1 μg/ml), human OX40L-Fc (5 μg/ml), and JAG1 + OX40L in the presence of IL-2 for 5 d, and frequencies of CD4$^+$CD25$^+$FOXP3$^+$ Tregs were analyzed. (**B**) Bar graph summarizes the frequencies of CD25$^+$FOXP3$^+$ Tregs. Values represent mean ± SEM, $n = 8$ independent experiments. **$p < 0.01$, ***$p < 0.005$ versus IL-2. (**C**) Human thymocytes were cultured with either IL-2 alone or OX40L + JAG1 + IL-2 for 5 d, and the proliferation of CD4$^+$Foxp3$^+$ and CD4$^+$Foxp3$^-$ cells was assayed by CellTrace Violet dilution. (**D**) The bar graph shows percentages of resting and proliferating CD4$^+$Foxp3$^+$ Tregs (values represent mean ± SEM, $n = 5$). *$p < 0.05$ versus IL-2. (**E**) Representative dot plots from the above experiments show the frequencies of CD45RA$^+$Foxp3^{low} (naive Tregs), CD45RA$^-$Foxp3^{hi} (effector Tregs), and CD45RA$^-$Foxp3^{low} (Teffs) in the culture. (**F**) Overlay histograms show the expression levels of Treg functional markers CTLA4, CD39, Helios, and TIGIT in CD4$^+$Foxp3^{hi} Tregs expanded from IL-2– (blue) versus OX40L + JAG1– (red) treated cultures. (**G**) In vitro Treg suppression assay was performed using autologous CD4$^+$CD25$^-$CD127^{high} Teffs and fresh/OX40L-JAG1–expanded CD4$^+$CD25^{hi}CD127^{low} Tregs in the presence of anti-CD3 stimulation for 4 d. The extent of Teff proliferation was measured by CellTrace Violet dilution assay. (**H**) Bar graphs show division index of Teffs calculated from each culture conditions. (**I**) NSG mice engrafted with human CD34 precursor cells were treated with soluble OX40L and JAG1. Representative dot plots show the development of human CD45$^+$CD4$^+$ T cells in humanized NSG mice. Representative dot plots and bar graphs show the frequencies of Foxp3^{hi} human Tregs within gated human CD45$^+$CD4$^+$ T cells in spleen (top panel) and liver of PBS versus OX40L-JAG1–treated mice. Values represent mean ± SEM, $n = 4$. *$p < 0.05$. (**J**) Bar graph shows the frequencies of CD45RA$^+$Foxp3^{low} (naive Tregs), CD45RA$^-$Foxp3^{hi} (effector Tregs), and CD45RA$^-$Foxp3^{low} (Teffs) within CD45$^+$CD4$^+$Foxp3$^+$ cells in PBS versus OX40L-JAG1–treated NSG mice. Values represent mean ± SEM, $n = 4$, *$p < 0.05$. (**K**) Overlay histogram analysis shows CTLA4 and TIGIT expression in CD45RA$^-$Foxp3^{hi} effector Tregs from PBS- versus OX40L-JAG1–treated NSG mice.

in thymus and spleen of OX40L-JAG1–cotreated mice compared with PBS-treated mice. These findings demonstrated the ability of OX40L-JAG1 treatment to induce Treg proliferation in vivo even under autoimmune conditions in NOD mice. In addition, we found a significant increase in CD4$^+$CD25$^-$Foxp3^{low} thymic Treg precursors and CD4$^+$CD25$^+$Foxp3$^+$ matured Tregs in OX40L-JAG1– treated mice, indicating the possible role of these ligands in thymic Treg differentiation as well. Furthermore, because the TCR-independent phase is an integral part of thymic Treg development, it is likely that OX40L and JAG1 contributed to increased

thymic output of Tregs by inducing both Treg differentiation and proliferation during that phase (16, 25).These findings are consistent with earlier reports of OX40 signaling enhancing IL-2–dependent thymic Treg maturation in a TCR-independent manner (25, 33).

One of the major hurdles associated with Treg therapy is the lineage stability of expanded Tregs. TSDR at Foxp3 gene locus allows for the constitutive expression of Foxp3, which is essential for the repression of TCR activation–induced inflammatory genes, like *Ifn-g* and *Il-2* expression in Tregs (9). Thus, loss/reduced expression of Foxp3 in Tregs renders them unstable, resulting in

the expression of proinflammatory genes, which can exacerbate autoimmune response (29, 34). It has been shown that repeated TCR stimulation during ex vivo expansion of Tregs can lead to increased methylation of the CpG islands of TSDR at Foxp3 gene locus in a subset of Tregs, resulting in loss of Foxp3 expression/lineage stability (7, 17). Accordingly, TGF-β has been shown to antagonize TCR-induced cell cycle–dependent recruitment of DNMT1 to Foxp3 locus and thereby helps maintain Foxp3 expression (35). In our differential gene expression microarray analysis, we observed a specific increase in the expression of DNMT1 in Tregs expanded by anti-CD3/CD28 but not in OX40L/JAG1–expanded or fresh Tregs, reiterating the TCR signaling requirement for DNMT1 upregulation (Fig. 2A). Moreover, we found that OX40L-JAG1–induced Treg proliferation occurred independent of canonical TCR signaling and was mediated specifically by noncanonical NF-κB activation. Our findings are consistent with recent studies that showed massive inflammation and impaired suppressive function in Tregs upon deletion of NF-kB2 in Tregs, indicating a key role for noncanonical NF-κB signaling in Treg homeostasis (36). Therefore, it is likely that the TCR-independent nature of OX40L-JAG1–induced Treg expansion might favor the epigenetic lineage stability of the expanded Tregs. In support of this notion, we found a stable expression of lineage stability markers CD25, Foxp3, Helios, CTLA4, and GITR in Tregs expanded in the thymus, spleen, and lymph nodes of NOD mice. Moreover, WGBS analysis showed stable demethylation marks in nTreg signatures genes, such as *Foxp3, Il-2ra, Ctla4, Ikzf2,* and *Ikzf4*, in OX40L-JAG1–expanded Tregs compared with control Tregs in the periphery, implying that OX40L-JAG1–expanded Tregs are lineage stable.

In the EAT model, we found OX40L-JAG1 treatment to increase functional Tregs in the thymus and periphery of CBA/j mice and alleviate EAT. This protective effect was accompanied by reduced thyroid lymphocytic infiltration, Th2 response, and autoantibody production. Among the expanded Tregs, we found a specific increase in subsets expressing elevated levels of coinhibitory receptors, such as CTLA4 and TIGIT, in the dLNs. These coinhibitory receptors are known to modulate APC functions through two independent coinhibitory signaling axes: CTLA4-CD28-CD80/CD86 and TIGIT-CD226-CD155/CD112 (37, 38). There was a modest increase in TIM3-expressing Tregs as well in the dLNs. Unlike CTLA4, which is constitutively expressed by Tregs and is critical for their function, TIGIT and TIM3 are expressed on a subset of Tregs, and TIGIT⁺/TIM3⁺ Tregs were functionally superior to TIGIT⁻/TIM3⁻ Tregs under autoimmune conditions (31, 37). In line with these findings, we noted enhanced Treg suppressive functions in OX40L-JAG1–expanded Tregs compared with control Tregs, and, more interestingly, Teffs from OX40L-JAG1–treated mice were more susceptible to Treg-mediated suppression (Fig. 4E–G).

Signaling through TNFSF receptors, including OX40, has been shown to impair Treg functions and render Teffs resistant to Treg-mediated suppression (39, 40). In contrast, we observed enhanced suppression by Tregs from OX40L-JAG1–treated mice. Earlier, we had seen OX40L treatment alone to expand "nonfunctional" Tregs in older NOD mice when the inflammatory responses had already unfolded (41), and cotreatment with JAG1 was necessary for the expansion of functional Tregs in older NOD mice (16). These observations indicated that although OX40 signaling is sufficient to induce Treg expansion, JAG1 cosignaling is essential to maintain suppressive function of Tregs. This is in accordance with the findings from other groups that showed Notch3 signaling to regulate Foxp3 transcription (42) and in vivo functions of nTregs (43).

Many encouraging immune interventions discovered in mice have failed in human trials, likely because of inherent differences between human versus murine systems. The majority of the human Treg studies have been carried out using PBMCs, which are strikingly different in their phenotype from Tregs present in the lymphoid organs, and very little is known about the expansion of Tregs in the human lymphoid organs (44). We observed preferential expression of OX40 on Tregs over Tconvs in human thymus and spleen, but not in PBMCs, indicating a role for this receptor in human Treg expansion in lymphoid organs. Moreover, unlike murine Tregs, human Tregs are highly heterogeneous and have substantial differences in their phenotype (45, 46). Despite these differences, we found selective expansion of human Tregs, but not Tconvs, in thymocyte cultures treated with OX40L-JAG1, and a major proportion of expanded Tregs were of CD45⁻Foxp3ʰⁱ effector Tregs and not CD45-Foxp3ˡᵒʷ effector memory–like cells. Moreover, the expanded Tregs expressed functional markers CTLA4 and TIGIT and showed comparable suppressive function to that of freshly isolated Tregs.

Furthermore, we observed increased Foxp3ʰⁱ Tregs in the liver, but not in the spleen, of humanized NSG mice treated with OX40L-JAG1. Lack of Treg increase in the spleen upon OX40L-JAG1 treatment could be in part explained by the lack of thymic selection in humanized NSG mice. Increase in human Tregs observed in the liver of OX40L-JAG1–treated mice indicates a potential hitherto unidentified site for Treg expansion. Given that the humanized NSG mice are not ideal to study human thymus Treg expansion in vivo, our findings are significant. Evolving humanized mouse models such as NSG.BLT (bone marrow–liver–thymus) mice might be more suitable to study the effect of OX40L-JAG1 treatment on human thymus Treg expansion (47). Collectively, our results show a novel (to our knowledge) and conserved mechanism of Treg homeostasis and have important implications for treating autoimmunity.

Acknowledgments

Disclosures

The authors have no financial conflicts of interest.

References

1. Sakaguchi, S., T. Yamaguchi, T. Nomura, and M. Ono. 2008. Regulatory T cells and immune tolerance. *Cell* 133: 775–787.
2. Josefowicz, S. Z., L. F. Lu, and A. Y. Rudensky. 2012. Regulatory T cells: mechanisms of differentiation and function. *Annu. Rev. Immunol.* 30: 531–564.
3. Tang, Q., K. J. Henriksen, M. Bi, E. B. Finger, G. Szot, J. Ye, E. L. Masteller, H. McDevitt, M. Bonyhadi, and J. A. Bluestone. 2004. In vitro-expanded antigen-specific regulatory T cells suppress autoimmune diabetes. *J. Exp. Med.* 199: 1455–1465.
4. Glick, A. B., A. Wodzinski, P. Fu, A. D. Levine, and D. N. Wald. 2013. Impairment of regulatory T-cell function in autoimmune thyroid disease. *Thyroid* 23: 871–878.
5. Bluestone, J. A., J. H. Buckner, M. Fitch, S. E. Gitelman, S. Gupta, M. K. Hellerstein, K. C. Herold, A. Lares, M. R. Lee, K. Li, et al. 2015. Type 1 diabetes immunotherapy using polyclonal regulatory T cells. *Sci. Transl. Med.* 7: 315ra189.
6. Grant, C. R., R. Liberal, G. Mieli-Vergani, D. Vergani, and M. S. Longhi. 2015. Regulatory T-cells in autoimmune diseases: challenges, controversies and--yet--unanswered questions. [Published erratum appears in 2015 *Autoimmun. Rev.* 14: 845–846.] *Autoimmun. Rev.* 14: 105–116.
7. Komatsu, N., K. Okamoto, S. Sawa, T. Nakashima, M. Oh-hora, T. Kodama, S. Tanaka, J. A. Bluestone, and H. Takayanagi. 2014. Pathogenic conversion of Foxp3+ T cells into TH17 cells in autoimmune arthritis. *Nat. Med.* 20: 62–68.
8. Sawant, D. V., and D. A. A. Vignali. 2014. Once a Treg, always a Treg? *Immunol. Rev.* 259: 173–191.

9. Ohkura, N., M. Hamaguchi, H. Morikawa, K. Sugimura, A. Tanaka, Y. Ito, M. Osaki, Y. Tanaka, R. Yamashita, N. Nakano, et al. 2012. T cell receptor stimulation-induced epigenetic changes and Foxp3 expression are independent and complementary events required for Treg cell development. *Immunity* 37: 785–799.

10. Chen, L., and D. B. Flies. 2013. Molecular mechanisms of T cell co-stimulation and co-inhibition. [Published erratum appears in 2013 *Nat. Rev. Immunol.* 13: 542. *Nat. Rev. Immunol.* 13: 227–242.

11. Bhattacharya, P., A. Gopisetty, B. B. Ganesh, J. R. Sheng, and B. S. Prabhakar. 2011. GM-CSF-induced, bone-marrow-derived dendritic cells can expand natural Tregs and induce adaptive Tregs by different mechanisms. *J. Leukoc. Biol.* 89: 235–249.

12. Zou, T., A. J. Caton, G. A. Koretzky, and T. Kambayashi. 2010. Dendritic cells induce regulatory T cell proliferation through antigen-dependent and -independent interactions. *J. Immunol.* 185: 2790–2799.

13. Gopisetty, A., P. Bhattacharya, C. Haddad, J. C. Bruno, Jr., C. Vasu, L. Miele, and B. S. Prabhakar. 2013. OX40L/Jagged1 cosignaling by GM-CSF-induced bone marrow-derived dendritic cells is required for the expansion of functional regulatory T cells. *J. Immunol.* 190: 5516–5525.

14. Earle, K. E., Q. Tang, X. Zhou, W. Liu, S. Zhu, M. L. Bonyhadi, and J. A. Bluestone. 2005. In vitro expanded human CD4+CD25+ regulatory T cells suppress effector T cell proliferation. *Clin. Immunol.* 115: 3–9.

15. Masteller, E. L., M. R. Warner, Q. Tang, K. V. Tarbell, H. McDevitt, and J. A. Bluestone. 2005. Expansion of functional endogenous antigen-specific CD4+CD25+ regulatory T cells from nonobese diabetic mice. *J. Immunol.* 175: 3053–3059.

16. Kumar, P., K. Alharshawi, P. Bhattacharya, A. Marinelarena, C. Haddad, Z. Sun, S. Chiba, A. L. Epstein, and B. S. Prabhakar. 2017. Soluble OX40L and JAG1 induce selective proliferation of functional regulatory T-cells independent of canonical TCR signaling. *Sci. Rep.* 7: 39751.

17. Hoffmann, P., T. J. Boeld, R. Eder, J. Huehn, S. Floess, G. Wieczorek, S. Olek, W. Dietmaier, R. Andreesen, and M. Edinger. 2009. Loss of FOXP3 expression in natural human CD4+CD25+ regulatory T cells upon repetitive in vitro stimulation. *Eur. J. Immunol.* 39: 1088–1097.

18. Shimizu, K., S. Chiba, K. Kumano, N. Hosoya, T. Takahashi, Y. Kanda, Y. Hamada, Y. Yazaki, and H. Hirai. 1999. Mouse jagged1 physically interacts with notch2 and other notch receptors. Assessment by quantitative methods. *J. Biol. Chem.* 274: 32961–32969.

19. Okamoto, Y., D. C. Douek, R. D. McFarland, and R. A. Koup. 2002. Effects of exogenous interleukin-7 on human thymus function. *Blood* 99: 2851–2858.

20. Gangi, E., C. Vasu, D. Cheatem, and B. S. Prabhakar. 2005. IL-10-producing CD4+CD25+ regulatory T cells play a critical role in granulocyte-macrophage colony-stimulating factor-induced suppression of experimental autoimmune thyroiditis. *J. Immunol.* 174: 7006–7013.

21. Vasu, C., R. N. Dogan, M. J. Holterman, and B. S. Prabhakar. 2003. Selective induction of dendritic cells using granulocyte macrophage-colony stimulating factor, but not fms-like tyrosine kinase receptor 3-ligand, activates thyroglobulin-specific CD4+/CD25+ T cells and suppresses experimental autoimmune thyroiditis. *J. Immunol.* 170: 5511–5522.

22. Ganesh, B. B., D. M. Cheatem, J. R. Sheng, C. Vasu, and B. S. Prabhakar. 2009. GM-CSF-induced CD11c+CD8a--dendritic cells facilitate Foxp3+ and IL-10+ regulatory T cell expansion resulting in suppression of autoimmune thyroiditis. *Int. Immunol.* 21: 269–282.

23. Courtney, A. H., W. L. Lo, and A. Weiss. 2018. TCR signaling: mechanisms of initiation and propagation. *Trends Biochem. Sci.* 43: 108–123.

24. Baeyens, A., D. Saadoun, F. Billiard, A. Rouers, S. Grégoire, B. Zaragoza, Y. Grinberg-Bleyer, E. Piaggio, and B. L. Salomon. 2015. Effector T cells boost regulatory T cell expansion by IL-2, TNF, OX40, and plasmacytoid dendritic cells depending on the immune context. *J. Immunol.* 194: 999–1010.

25. Kumar, P., A. Marinelarena, D. Raghunathan, V. K. Ragothaman, S. Saini, P. Bhattacharya, J. Fan, A. L. Epstein, A. V. Maker, and B. S. Prabhakar. 2019. Critical role of OX40 signaling in the TCR-independent phase of human and murine thymic Treg generation. *Cell. Mol. Immunol.* 16: 138–153.

26. Vail, M. E., M. L. Chaisson, J. Thompson, and N. Fausto. 2002. Bcl-2 expression delays hepatocyte cell cycle progression during liver regeneration. *Oncogene* 21: 1548–1555.

27. Zinkel, S., A. Gross, and E. Yang. 2006. BCL2 family in DNA damage and cell cycle control. *Cell Death Differ.* 13: 1351–1359.

28. Chen, K., Y. Wei, G. C. Sharp, and H. Braley-Mullen. 2001. Induction of experimental autoimmune thyroiditis in IL-12-/- mice. *J. Immunol.* 167: 1720–1727.

29. Wang, J., A. Ioan-Facsinay, E. I. van der Voort, T. W. Huizinga, and R. E. Toes. 2007. Transient expression of FOXP3 in human activated nonregulatory CD4+ T cells. *Eur. J. Immunol.* 37: 129–138.

30. Kmieciak, M., M. Gowda, L. Graham, K. Godder, H. D. Bear, F. M. Marincola, and M. H. Manjili. 2009. Human T cells express CD25 and Foxp3 upon activation and exhibit effector/memory phenotypes without any regulatory/suppressor function. *J. Transl. Med.* 7: 89.

31. Kumar, P., P. Bhattacharya, and B. S. Prabhakar. 2018. A comprehensive review on the role of co-signaling receptors and Treg homeostasis in autoimmunity and tumor immunity. *J. Autoimmun.* 95: 77–99.

32. Au-Yeung, B. B., J. Zikherman, J. L. Mueller, J. F. Ashouri, M. Matloubian, D. A. Cheng, Y. Chen, K. M. Shokat, and A. Weiss. 2014. A sharp T-cell antigen receptor signaling threshold for T-cell proliferation. *Proc. Natl. Acad. Sci. USA* 111: E3679–E3688.

33. Mahmud, S. A., L. S. Manlove, H. M. Schmitz, Y. Xing, Y. Wang, D. L. Owen, J. M. Schenkel, J. S. Boomer, J. M. Green, H. Yagita, et al. 2014. Costimulation via the tumor-necrosis factor receptor superfamily couples TCR signal strength to the thymic differentiation of regulatory T cells. *Nat. Immunol.* 15: 473–481.

34. Miyara, M., Y. Yoshioka, A. Kitoh, T. Shima, K. Wing, A. Niwa, C. Parizot, C. Taflin, T. Heike, D. Valeyre, et al. 2009. Functional delineation and differentiation dynamics of human CD4+ T cells expressing the FoxP3 transcription factor. *Immunity* 30: 899–911.

35. Josefowicz, S. Z., C. B. Wilson, and A. Y. Rudensky. 2009. Cutting edge: TCR stimulation is sufficient for induction of Foxp3 expression in the absence of DNA methyltransferase 1. *J. Immunol.* 182: 6648–6652.

36. Grinberg-Bleyer, Y., R. Caron, J. J. Seeley, N. S. De Silva, C. W. Schindler, M. S. Hayden, U. Klein, and S. Ghosh. 2018. The alternative NF-κB pathway in regulatory T cell homeostasis and suppressive function. *J. Immunol.* 200: 2362–2371.

37. Anderson, A. C., N. Joller, and V. K. Kuchroo. 2016. Lag-3, Tim-3, and TIGIT: co-inhibitory receptors with specialized functions in immune regulation. *Immunity* 44: 989–1004.

38. Walker, L. S. 2013. Treg and CTLA-4: two intertwining pathways to immune tolerance. *J. Autoimmun.* 45: 49–57.

39. Takeda, I., S. Ine, N. Killeen, L. C. Ndhlovu, K. Murata, S. Satomi, K. Sugamura, and N. Ishii. 2004. Distinct roles for the OX40-OX40 ligand interaction in regulatory and nonregulatory T cells. *J. Immunol.* 172: 3580–3589.

40. Barsoumian, H. B., E. S. Yolcu, and H. Shirwan. 2016. 4-1BB signaling in conventional T cells drives IL-2 production that overcomes CD4+CD25+FoxP3+ T regulatory cell suppression. *PLoS One* 11: e0153088.

41. Haddad, C. S., P. Bhattacharya, K. Alharshawi, A. Marinelarena, P. Kumar, O. El-Sayed, H. A. Elshabrawy, A. L. Epstein, and B. S. Prabhakar. 2016. Age-dependent divergent effects of OX40L treatment on the development of diabetes in NOD mice. *Autoimmunity* 49: 298–311.

42. Barbarulo, A., P. Grazioli, A. F. Campese, D. Bellavia, G. Di Mario, M. Pelullo, A. Ciuffetta, S. Colantoni, A. Vacca, L. Frati, et al. 2011. Notch3 and canonical NF-kappaB signaling pathways cooperatively regulate Foxp3 transcription. *J. Immunol.* 186: 6199–6206.

43. Campese, A. F., P. Grazioli, S. Colantoni, E. Anastasi, M. Mecarozzi, S. Checquolo, G. De Luca, D. Bellavia, L. Frati, A. Gulino, and I. Screpanti. 2009. Notch3 and pTalpha/pre-TCR sustain the in vivo function of naturally occurring regulatory T cells. *Int. Immunol.* 21: 727–743.

44. Nagar, M., J. Jacob-Hirsch, H. Vernitsky, Y. Berkun, S. Ben-Horin, N. Amariglio, I. Bank, Y. Kloog, G. Rechavi, and I. Goldstein. 2010. TNF activates a NF-kappaB-regulated cellular program in human CD45RA- regulatory T cells that modulates their suppressive function. *J. Immunol.* 184: 3570–3581.

45. Rudensky, A. Y. 2011. Regulatory T cells and Foxp3. *Immunol. Rev.* 241: 260–268.

46. Sakaguchi, S., M. Miyara, C. M. Costantino, and D. A. Hafler. 2010. FOXP3+ regulatory T cells in the human immune system. *Nat. Rev. Immunol.* 10: 490–500.

47. Smith, D. J., L. J. Lin, H. Moon, A. T. Pham, X. Wang, S. Liu, S. Ji, V. Rezek, S. Shimizu, M. Ruiz, et al. 2016. Propagating humanized BLT mice for the study of human immunology and immunotherapy. *Stem Cells Dev.* 25: 1863–1873.